Proc. Natl. Acad. Sci. USA
Vol. 94, pp. 12263–12267, November 1997
Geology

Third-generation synchrotron x-ray diffraction of 6-μm crystal of raite, $\approx Na_3Mn_3Ti_{0.25}Si_8O_{20}(OH)_2 \cdot 10H_2O$, opens up new chemistry and physics of low-temperature minerals

(crystal structure/microcrystal/phyllosilicate)

JOSEPH J. PLUTH*, JOSEPH V. SMITH*†, DMITRY Y. PUSHCHAROVSKY‡, EUGENII I. SEMENOV§, ANDREAS BRAM¶, CHRISTIAN RIEKEL¶, HANS-PETER WEBER¶, AND ROBERT W. BROACH‖

*Department of Geophysical Sciences, Center for Advanced Radiation Sources, Geological/Soil/Environmental, and Materials Research Science and Engineering Center, 5734 South Ellis Avenue, University of Chicago, Chicago, IL 60637; ‡Department of Geology, Moscow State University, Moscow, 119899, Russia; §Fersman Mineralogical Museum, Russian Academy of Sciences, Moscow, 117071, Russia; ¶European Synchrotron Radiation Facility, BP 220, 38043, Grenoble, France; and UOP Research Center, Des Plaines, IL 60017

Contributed by Joseph V. Smith, September 3, 1997

ABSTRACT **The crystal structure of raite was solved and refined from data collected at Beamline Insertion Device 13 at the European Synchrotron Radiation Facility, using a 3 × 3 × 65 μm single crystal. The refined lattice constants of the monoclinic unit cell are a = 15.1(1) Å; b = 17.6(1) Å; c = 5.290(4) Å; β = 100.5(2)°; space group $C2/m$. The structure, including all reflections, refined to a final R = 0.07. Raite occurs in hyperalkaline rocks from the Kola peninsula, Russia. The structure consists of alternating layers of a hexagonal chicken-wire pattern of 6-membered SiO_4 rings. Tetrahedral apices of a chain of Si six-rings, parallel to the c-axis, alternate in pointing up and down. Two six-ring Si layers are connected by edge-sharing octahedral bands of Na^+ and Mn^{3+} also parallel to c. The band consists of the alternation of finite Mn–Mn and Na–Mn–Na chains. As a consequence of the misfit between octahedral and tetrahedral elements, regions of the Si–O layers are arched and form one-dimensional channels bounded by 12 Si tetrahedra and 2 Na octahedra. The channels along the short c-axis in raite are filled by isolated $Na(OH,H_2O)_6$ octahedra. The distorted octahedrally coordinated Ti^{4+} also resides in the channel and provides the weak linkage of these isolated Na octahedra and the mixed octahedral tetrahedral framework. Raite is structurally related to intersilite, palygorskite, sepiolite, and amphibole.**

Natural processes selected some 4,000 known mineral species (Nomenclature Committee of the International Mineralogical Association), of which several hundred have industrial applications. Most occur at the Earth's surface. The crystal structures of minerals are the key to understanding chemical and physical processes on Earth, and for testing remote observations and ideas on the Solar System and Universe. Agriculture, the energy and metal industries, hydrology, and geobiology, in particular, are based on chemical reactions in and on micrometer mineral grains. The petroleum and chemical industries use zeolite catalysts (1), many of which are analogous with the rare mineral faujasite. All advances in scientific technology permit new science, and indeed should be driven thereby. About one-fifth of known minerals lack a structure determination,** mainly because crystals are too small or imperfect for laboratory x-ray sources. This determination of the crystal structure of raite by using x-rays from a third-generation synchrotron source opens the gate to a new field of microgeochemistry, which has important applications to agriculture, the energy and metal industries, hydrology, and geobiology. Raite lies in the chemical cooling sequence of exotic hyperalkaline rocks of the Kola Peninsula, Russia, and the Monteregian Hills, Canada (2). This hydrated sodium-manganese silicate extends the already wide range of manganese crystal chemistry (3), which includes various complex oxides in ore deposits and nodules from the sea floor and certain farming areas, the pyroxmangite analog of the lunar volcanic metasilicate pyroxferroite, the Mn analog yofortierite of the clay mineral palygorskite, and the unnamed Mn analog of sepiolite.

Historically, crystal chemistry began with the determination of the atomic packings in centimeter to millimeter crystals of minerals such as halite and diamond some 80 years ago, using primitive x-ray sources and detectors (Bragg era). It moved on to more complex structures in the 1920s and 1930s (era of Pauling, Taylor, and other crystal chemists) as hot-cathode x-ray machines became powerful enough for submillimeter crystals. By the 1960s, new mathematical techniques coupled with the most intense laboratory x-ray sources and sensitive detectors allowed structure determination of single crystals down to about 0.05 mm, leading to comprehensive crystal-chemical reviews (4–7). In the 1970s, the available x-ray intensity began to increase dramatically as "synchrotron" radiation was extracted from bending magnets of synchronized accelerators originally designed for high-energy physics. New generations of dedicated synchrotron sources are providing further advances in the intensity and particularly the quality [narrow angular divergence and energy spread; controlled polarization; tunability from high (100 keV) to low energy]. The third-generation synchrotron x-ray sources are designed around multi-magnet insertion devices ("undulators" and "wigglers"). The European Synchrotron Research Facility (ESRF) in Grenoble, France (operational), the Advanced Photon Source in Argonne, Illinois (commissioning), and the Super Photon Ring-8 in Harima Science Garden City, Japan (commissioning), permit various types of microanalysis (8), including determination of the crystal structure of micrometer single crystals, when beamlines are fully optimized by subtle improvements in x-ray focusing, data collection, and computer processing. Second-generation synchrotron x-ray beams have revolutionized the determination of a crystal structure from a near-random powder of pure, well-crystallized material (9),

Abbreviation: ESRF, European Synchrotron Radiation Facility.

†To whom reprint requests should be addressed. e-mail: smith@geo1.uchicago.edu.

**See *Crystal Structures of Minerals and Chemical Analogs*, an unpublished database updated weekly, compiled by J.V.S. at the University of Chicago. Requests on specific minerals answered at smith@geo1.uchicago.edu.

The publication costs of this article were defrayed in part by page charge payment. This article must therefore be hereby marked "*advertisement*" in accordance with 18 U.S.C. §1734 solely to indicate this fact.

but they lack the brilliance needed to determine the structure of a single crystal selected from the powder. Impure samples of a poorly crystallized phase require single-crystal diffraction studies using third-generation synchrotron x-ray sources coupled with other techniques, including electron diffraction/microscopy and various spectroscopies. The third-generation insertion devices provide x-ray beams intense enough for study of single crystals somewhat smaller than 1 μm.

Current progress in recording diffraction data for small crystals is reviewed by Harding (10). Monochromatic data recorded on a FAST "conventional" diffractometer has permitted structure determination for crystals as small as 20–40 μm, corresponding to crystal volume × scattering power of $\approx 5 \times 10^{12}$ e^2·Å^{-3}. Usable synchrotron diffraction data have been obtained from various crystals less than 1 μm^3, including a study of thin plates of kaolinite at ESRF (11).

There are problems with the interpretation of diffuse diffraction streaks from small crystals such as the kaolinite plates. Such thin plates, and also narrow needles, may have insufficient scatterers along the short directions. More complex and challenging is to evaluate diffuse scattering in terms of the chemical and physical changes at the surface, where the atomic environment must be different from the interior. Careful control of the humidity will be neeeded for study of micrometer crystals that respond to hydrogen bonding. Even a microcrystal of diamond must have some type of termination for the projecting electron orbitals, perhaps hydrogen or oxygen.

Hence a growing challenge for study of micrometer minerals is to find ones sufficiently well crystallized that the advances in synchrotron technology can be harnessed to geochemical purposes. We deliberately selected raite because its optically perfect microneedles (3 × 3 × 65 μm; compare diameter of human hair, ≈60 μm) promised to yield important crystal-chemical information. The 3-μm width was large enough for sharp diffractions. To optimize the signal-to-noise ratio on the ESRF Beamline Insertion Device 13, the crystal was irradiated with a 30-μm focused x-ray beam, but there would have been enough intensity for a much smaller beam (12). Indeed, one can envisage multispot structure determination with a circular micrometer beam using an egg crate raster or a tomographic deconvolution, or even more fancy using a hollow beam just wide enough to accentuate the surface structure. For a mineral needle, one can envisage measurement of crystal-chemical changes responding to evolution of geological processes as the needle grew.

Raite (13), originally given as $Na_4Mn_3Si_8(O,OH)_{24}\cdot 9H_2O$, occurs with 11 other new minerals and 40 known ones, in the Yubileinaya pegmatite vein cutting agpaitic (= excess alkali) nepheline syenite at Karnasurt Mountain, Lovozero alkaline massif, Kola peninsula (2). The name honors Thor Heyerdahl's Pacific voyage on the raft *Ra*. The deep-seated vein, which lies between foyaite (nepheline syenite richer in potassium feldspar than nepheline) and underlying lujavrites (eudialyte-bearing nepheline syenite with interstitial nepheline and acmite needles between thin feldspar plates), has mineral assemblages classified as primary pegmatitic, early hydrothermal, late hydrothermal, and epithermal. In the last epithermal stage, earlier minerals were replaced (e.g., vuonnemite by nenadkevichite and zorite), villiaumite was leached, and the cavities became lined with new generations of natrolite, aegirine, and albite, together with penkvilksite, raite, zorite, mountainite, ilmajokite, and galena. Golden needles of raite, up to 1–2 mm long and 0.02–0.04 mm across, form radial aggregates; perfect cleavage, parallel to (100), (010), and (001); Mohs hardness 3. Conventional oscillation/de Jong–Bouman diffraction photography (13) had yielded a few diffractions incorrectly attributed to an orthorhombic cell: a = 30.6(1) Å, b = 5.31(2) Å, c = 18.20(5) Å, $C222_1$.

MATERIALS AND METHODS

A single crystal with dimensions 3 × 3 × 65 μm^3, on a glass fiber tapered to 1 μm, was mounted on a single-crystal κ-geometry diffractometer at the ESRF (11). An x-ray beam from an undulator was focused to 30 μm by an ellipsoidal mirror, and monochromatized to 0.6883 Å (18 keV) by a channel-cut Si(111) crystal cooled by liquid nitrogen. Only half the volume or about 300 μm^3 of the crystal was actually irradiated. Seventy-three frames were collected on a charged-coupled area detector (11-cm fluorescent screen with lens coupling) by rotating ϕ 10° in 20 sec.

The DENZO program (14) yielded refined lattice constants of the monoclinic unit cell: a = 15.1(1) Å; b = 17.6(1) Å; c = 5.290(4) Å; β = 100.5(2)°; V = 1382.33 Å^3; space group $C2/m$. SHELXTL (15) yielded solution and refinement of the crystal structure by using 6,599 reflections merged to 1,164 unique reflections: R(merge) = 0.05; R = 0.07. The final difference Fourier map was featureless: $\delta\rho$ maximum and minimum were 0.98 e/Å^3 and −0.82 e/Å^3. Of the 3,080 reflections that should be absent from C-centering, 325 were observed weakly above 1 σ. Refinement in $P2/m$ yielded essentially the same structure. Possible ordering of Ti in a weakly occupied site, or an intergrowth of raite with a second phase, needs further study.

Qualitative x-ray emission analysis of the needle with a Cameca SX-50 electron microprobe confirmed the major Mn, Na, Si, and minor Ti in the original three bulk chemical analyses. Quantitative electron-probe analysis was ruled out by decomposition in the electron beam. A small peak located in final refinement refined to ≈11% Ti, inside the range of 1.4, 2.9, and 3.1 wt % TiO_2 from three conventional chemical analyses. The program MISSYM (16) did not reveal pseudosymmetry. Calculation of the sum of the bond strength on the anions (17) allowed assignment of O, OH, and H_2O to oxygen positions. The valence state of Mn is somewhat uncertain, but bond-strength modeling and the light honey color indicate mainly Mn^{2+}, and possibly some Mn^{3+}. Synchrotron absorption spectroscopy should yield quantitative information. In the meantime, the tentative structural formula, $Na_3(Mn^{2+})_3(Ti^{4+})_{0.25}[Si_8O_{20}](OH)_2\cdot 10H_2O$, and calculated density 2.39 g/cm^3 essentially match the original bulk chemical analyses and experimental density (13). The atomic coordinates and selected interatomic distances are collected in Table 1 and Table 2.

Table 1. Raite positional parameters

Atom	x	y	z	U_{eq}
Mn(1)	0.0	0.0	0.0	0.013(1)
Mn(2)	0.5	0.40289(8)	0.5	0.017(1)
Na(1)	0.5	0.2997(2)	0.0	0.019(2)
Na(2)	0.5	0.0	0.0	0.040(3)
Ti*	0.5	0.2039(10)	0.5	0.025(8)
Si(1)	0.31210(12)	0.41406(9)	0.0569(5)	0.010(1)
Si(2)	0.30524(12)	0.32828(9)	0.5497(5)	0.011(1)
O(1)	0.4198(3)	0.4133(2)	0.1184(12)	0.016(2)
O(2)	0.0882(3)	0.1816(3)	0.4077(13)	0.021(2)
O(3)	0.25	0.25	0.5	0.028(3)
O(4)†	0.0678(5)	0.0	0.361(2)	0.020(3)
O(5)	0.2718(4)	0.5	0.006(2)	0.012(3)
O(6)	0.2295(3)	0.1328(3)	0.2036(12)	0.013(2)
O(7)	0.2686(3)	0.3802(3)	0.2936(12)	0.014(2)
O(8)‡	0.4018(6)	0.0	0.304(2)	0.042(4)
O(9)‡	0.0720(5)	0.3992(4)	0.271(2)	0.054(3)
O(10)‡	0.4176(6)	0.2096(4)	0.201(2)	0.062(4)

*Occupancy O 0.45(4) atoms per unit cell.
†OH.
‡H_2O.

Table 2. Bond lengths

Bond	Length, Å	Bond	Length, Å
2Mn(1)—O(4)	1.998(10)	2Mn(2)—O(2)	2.112(10)
4Mn(1)—O(1)	2.112(9)	2Mn(2)—O(1)	2.164(8)
2Na(1)—O(2)	2.342(9)	2Mn(2)—O(4)	2.186(10)
2Na(1)—O(10)	2.382(11)	2Na(2)—O(8)	2.376(14)
2Na(1)—O(1)	2.477(12)	4Na(2)—O(9)	2.412(12)
2Ti—O(10)	1.828(13)	2Ti—O(2)	2.512(19)
2Ti—O(9)	2.534(18)	Si(2)—O(2)	1.593(12)
Si(1)—O(1)	1.600(12)	Si(2)—O(3)	1.607(7)
Si(1)—O(7)	1.628(7)	Si(2)—O(6)	1.642(7)
Si(1)—O(6)	1.631(7)	Si(2)—O(7)	1.645(7)
Si(1)—O(5)	1.634(9)		

RESULTS AND DISCUSSION

A *c*-axis projection (Fig. 1*A*) shows how corrugated layers of SiO_4 tetrahedra (shaded triangles) are reflected in (010) and linked by layers of Na and Mn octahedra. Fig. 1*B* shows the hexagonal "chicken-wire" pattern of a layer of composition Si_2O_5. Triangles containing spokes represent tetrahedra pointing up, and empty ones represent tetrahedra pointing down. This layer can be described as sinusoidal strings of triangles ["zweier single chains" in the nomenclature of Liebau (6)] generating vertex-sharing six-rings of tetrahedra of "equal directedness," parallel to *c*, pointing up (triangles containing spokes) and down (empty) alternatively along the *b*-axis (Fig. 1*A*). These adjacent six-ring chains point in the opposite direction to generate a corrugated layer by "tetrahedral inversion." This layer also occurs in palygorskite (18–20), $Mg_5[Si_8O_{20}](OH)_2{\cdot}8H_2O$ (idealized formula) and almost certainly in yofortierite (21), $Mn_5[Si_8O_{20}](OH)_2{\cdot}8H_2O$.

Two six-ring Si bands from adjacent layers are bridged by edge-sharing octahedral bands of Na and (mainly) Mn^{2+} (Fig. 1*A*) formed by the alternation (Fig. 1*C*) of finite edge-sharing Na(1)–Mn(1)–Na(1) and Mn(2)–Mn(2) octahedra. Geometrical misfit between the octahedral and tetrahedral elements forces arching of the Si–O layers. The resultant one-dimensional channels are bounded by 12 Si tetrahedra and 2 Na and filled by isolated NaO_6 octahedra. The weakly occupied Ti^{4+} site (Fig. 1*C*) also resides in the channel, and its tetragonal bipyramidal bonding matches that in lindsleyite (22). Its structural role in linking Na octahedra to the mixed octahedral–tetrahedral framework needs further study.

The geometrical matching between the various structural units is very important in determining the specific topology of complex low-temperature minerals, including clay minerals. Thus the misfit between tetrahedral silicate layers and octahedral M-cation layers results in curvature and inversion of various types (23). Very few crystal structures have been determined with enough accuracy to allow quantitative testing of geometrical models, and many published layer and band structures are based on idealized "flat'" components. In particular, the structural models of palygorskite and sepiolite (24) are idealized. The raite structure illustrates the importance of inversion and curvature in accommodating structural misfit between the silicate layer and the Mn octahedral band. Some minor accommodation can be expected with the band of Na-octahedra and water.

Selected relationships between raite and other structures with tetrahedral inversion or octahedral Mn are shown in Fig. 2; other relationships will be published elsewhere. In sepiolite (25, 26) and its unnamed Mn analog, inversion takes place after three zweier single chains (Fig. 2*A*). The amphibole ungarettiite (27), $Na_3Mn_2^{2+}Mn_3^{3+}Si_8O_{22}O_2$, has tetrahedron inversion (Fig. 2*B*) between isolated neighboring bands $[Si_4O_{11}]$.

Intersilite (28–30), $(Na,K)Na_5Mn(Ti,Nb)[Si_{10}O_{24}(OH)](O,OH)(OH)_2{\cdot}4H_2O$ (not shown), has silicate layers with 8-, 6-, and 5-membered rings. Tension is relieved by reversing two tetrahedra in each 8-membered ring. Like raite, intersilite has a band of Na octahedra that fit neatly with the dominant octahedral/tetrahedral bonding complex.

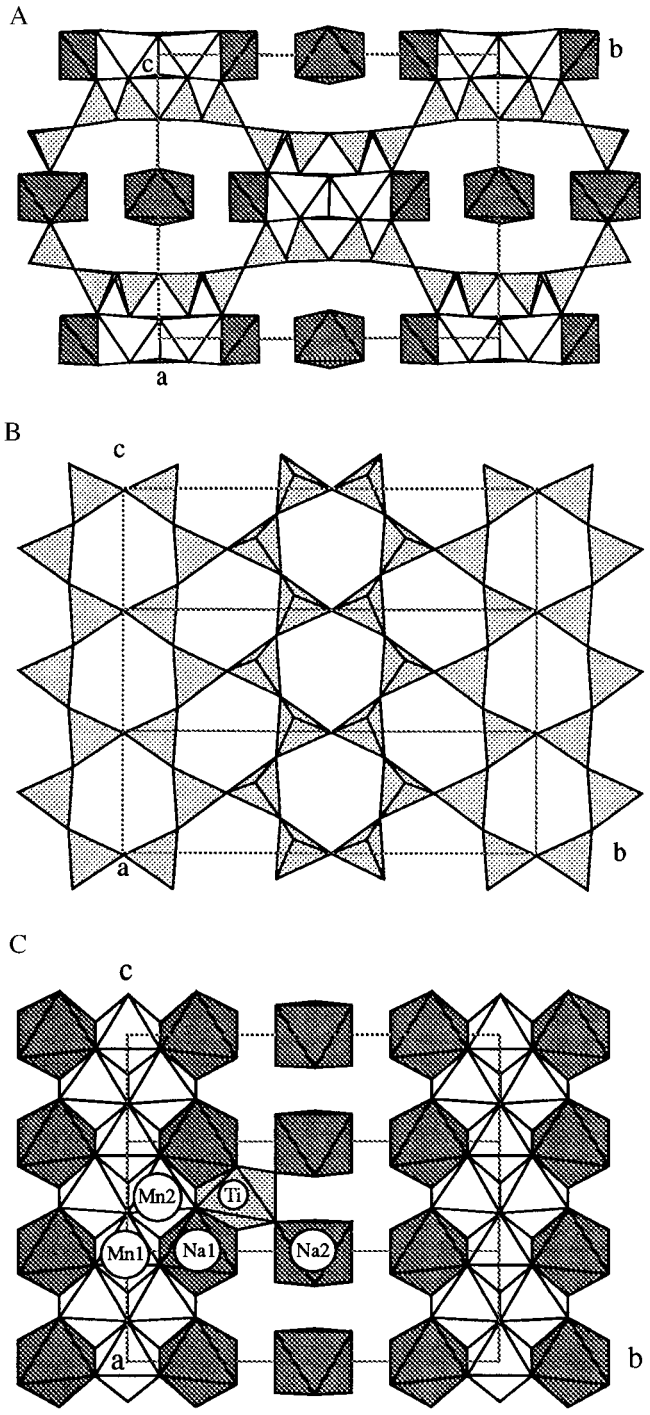

FIG. 1. Crystal structure of raite. (*A*) Down the *c*-axis: triangles, SiO_4 tetrahedra; white octahedra, Mn; shaded octahedra, Na. (*B*) SiO_4 layer projected down *a*, at $z \approx 0$. (*C*) Mn and Na polyhedra down *a*; the Ti octahedron (dotted) has one-ninth occupancy.

The theoretical structure model of the new silicate kalifersite (31), $(K,Na)_5Fe_7^{3+}[Si_{20}O_{50}(OH)_6]{\cdot}12H_2O$, from a hydrothermally altered pegmatite of the Khibina massif (Kola peninsula, Russia), also contains a tetrahedrally inverted silicate layer, here with alternating palygorskite- and sepiolite-like ribbons (not shown).

The raite and palygorskite structures (24) differ mainly in that the octahedral site at the origin is unoccupied in paly-

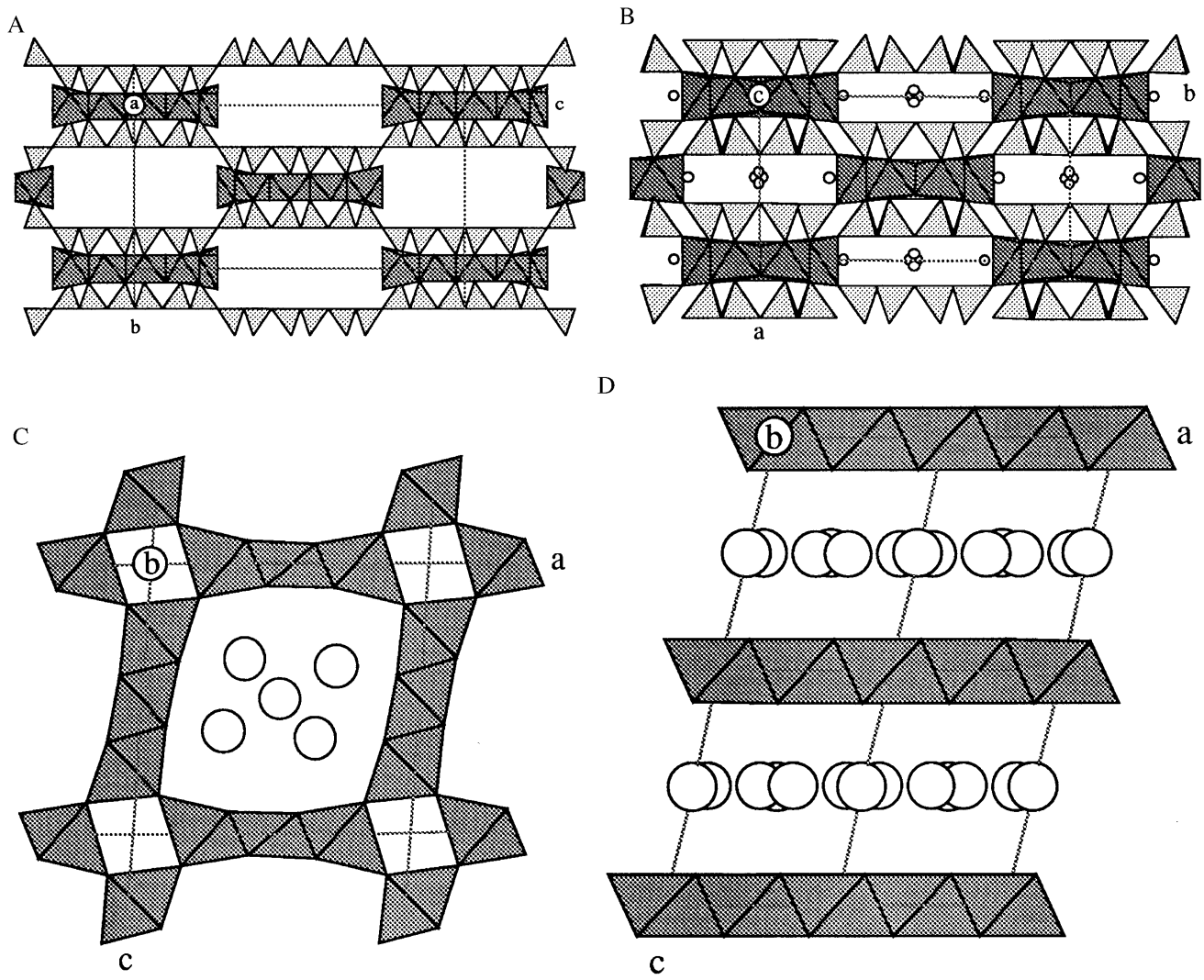

FIG. 2. Representative examples of structures containing Mn (shaded octahedra). Sepiolite and ungarettiite also contain SiO_4 tetrahedra (triangles). (*A*) Sepiolite. Idealized model showing tetrahedral inversion with six "up" and six "down" triangles. The pentuple bands of edge-shared Mg octahedra flare out to accommodate the weaker bonding to water molecules in the rectangular gaps. (*B*) Ungarettiite, a member of the amphibole mineral family. Refined model showing the inversion of trapezium-shaped bands of silica tetrahedra, and the cross-linking of the triple bands of Mn octahedra. Small circles next to the Mn are Na. Subtle structural complexities are related to the mainly trivalent valency of Mn. (*C*) Todorokite. Edge-shared triple-octahedral bands are vertex-linked around tetragonal tunnels in this 3×3 structure type. There are many stacking variants starting with the 1×1 type in rutile. The circles represent positions occupied by Na and water not differentiated in a structural model fitted to x-ray powder diffraction data. (*D*) Birnessite. An example of Mn octahedral layers linked together by Na and water (undifferentiated circles).

gorskite when the chemical composition is $Mg_2Al_2[Si_8O_{20}](OH)_2{\cdot}8H_2O$ and only four rather than five cations are present. The tunnels along the short *c*-axis in raite are filled by isolated $Na_2(H_2O)_6$ octahedra, whereas those in palygorskite accommodate only water molecules. Accurate structure determination of the various types of palygorskite (and sepiolite) is desirable to evaluate the extent of deviation from idealized flat geometry.

To conclude, we set raite in the general scheme of mineral geochemistry of manganese. The variation of valence state from divalent to trivalent to tetravalent is extremely important for understanding the range of crystal structures among the 345 named minerals containing Mn as the dominant ion in at least one site. Most of the earth is sufficiently reduced for Mn^{2+} to associate with dominant Fe^{2+}. In the crust and upper mantle, divalent manganese mainly occurs in atomic positions dominated by divalent iron, as in garnets, olivines, pyroxenes (namansilite), amphiboles, etc. Rarely, Mn dominates a crystallographic site in silicates as in pyroxenes (donpeacorite, kanoite, and namansilite) and amphiboles (e.g., kozulite, manganocummingtonite, and ungarettiite; but note trivalent Mn in kornite), etc. Under oxidizing conditions near the Earth's surface, manganese becomes partly trivalent or tetravalent, and there is a complex linkage with geological conditions (32). Thus, in nodules on the ocean floor, and in various special environments, manganese oxides (3, 33) occur as tunnel structures bounded by edge-sharing octahedral walls; examples are coronadite (not shown), romanechite (not shown), and todorokite (Fig. 2*C*). Birnessite (Fig. 2*D*) and pennantite (not shown) contain sheets, rather than chains, of octahedrally coordinated Mn. Synthetic analogs of these minerals are being explored for catalytic applications, including the Octahedral Molecular Sieve Number 1 (34) with a 3×3 tunnel structure analogous to todorokite.

In agriculture, divalent manganese from fluids in cells is converted into a black smut (quadrivalent manganese oxide) (35) by various bacteria, including the ones responsible for "take-all" disease in wheat. Similar oxidation processes occur in fungal diseases of trees (36). Biological evolution may have originated from iron monosulfide bubbles at a redox/pH front

driven by hydrothermal activity on the sea floor (37). Perhaps manganese might also be involved because of its ready utilization by modern bacteria. Microcrystallography of biological manganese compounds might prove useful in further characterization of the reaction mechanisms.

Finally, the high precision of the atomic coordinates of raite offers hope that synchrotron microcrystallography will provide a way of accurately characterizing structural features, such as the curvature of the bands and the hydrogen bonding, in many poorly defined minerals and their ion-exchanged derivatives. The next technical challenge is to move on from crystals that have enough scattering elements for generation of sharp Bragg diffractions to smaller ones in which surface features can be interpreted from non-Bragg diffractions. Further on will be actual-time chemistry in which ion-exchange and molecular absorption are monitored from the synchrotron x-ray diffraction.

We thank Ian Steele for electron microprobe analyses; the Russian Scientific Foundation (Grant 97-05-64000) and the Russian Universities Programme; the funding agencies responsible for the construction and operation of the ESRF; UOP; and the funding agencies supporting the Center for Advanced Radiation Sources Geological/Soil/Environmental, especially the National Science Foundation (Principal Investigator, Mark L. Rivers) and the Department of Energy (Principal Investigator, Stephen R. Sutton). J.J.P. thanks the Materials Research Science and Engineering Center at the University of Chicago (Grant NSF-DMR-00379). H.P.W. acknowledges financial support from the Swiss National Science Foundation (Grant 20-46928.96). J.V.S. particularly thanks many staff members at the Synchrotron Radiation Source, Daresbury, U.K., and the National Synchrotron Light Source, Brookhaven, NY, for technical discussions over the past decade.

1. Flanigen, E. M. (1991) *Stud. Surf. Sci. Catal.* **58,** 13–34.
2. Khomyakov, A. P. (1995) *Mineralogy of Hyperagpaitic Alkaline Rocks* (Clarendon, Oxford).
3. Waychunas, G. A. (1991) *Rev. Mineral.* **25,** 11–68.
4. Bragg, W. L., Claringbull, G. F. & Taylor W. H. (1965) *The Crystal Structures of Minerals* (Bell, London).
5. Wells, A. F. (1991) *Structural Inorganic Chemistry* (Clarendon, Oxford), corrected 5th Ed.
6. Liebau, F. (1985) *Structural Chemistry of Silicates* (Springer, Berlin).
7. O'Keeffe, M. & Hyde, B. G. (1996) *Crystal Structures. I. Patterns and Symmetry* (Mineralogical Soc. Am., Washington, DC).
8. Smith, J. V. & Rivers, M. L. (1995) in *Microprobe Techniques in the Earth Sciences*, eds. Potts, P. J., Bowles, J. F. W., Reed, S. J. B. & Cave, M. R. (Chapman & Hall, London), pp. 163–233.
9. International Union of Crystallography (1996) *Collected Abstracts of the 17th Congress and General Assembly: Acta Crystallogr. A* **52,** Suppl.
10. Harding, M. M. (1996) *J. Synchrotron Rad.* **3,** 250–259.
11. Neder, R. B., Burghammer, M., Grasl, T., Schulz, H., Bram, A., Fiedler, S. & Riekel, C. (1977) *Z. Kristallogr.* **211,** 763–765.
12. Engstrom, P., Fiedler, S. & Riekel, C. (1995) *Rev. Sci. Instrum.* **66,** 1348–1350.
13. Mer'kov, A. N., Bussen, I. V., Goiko, E. A., Kulchitskaya, E. A., Men'shikov, Yu. P. & Nedorezov, A. P. (1973) *Zap. Vses. Mineral. Ova.* **102,** 54–62.
14. Otwinowski, Z. (1993) in *Data Collection and Processing*, eds. Sawyer, L., Isaacs. N. & Bailey, S. (Daresbury Lab., Warrington, U.K.), pp. 56–62.
15. Sheldrick, G. M. (1993) SHELXTL, Program for the Solution and Refinement of Crystal Structures (Siemens Energy and Automation, Madison, WI).
16. Le Page, Y. (1988) *J. Appl. Crystallogr.* **21,** 983–984.
17. Brown, I. D. & Shannon, R. D. (1973) *Acta Crystallogr. A* **29,** 266–282.
18. Drits, V. A. & Sokolova, G. V. (1971) *Soviet Phys. Crystallogr.* **16,** 183–185.
19. Chisholm, J. E. (1992) *Can. Mineral.* **30,** 61–63.
20. Artioli, G., Galli, E., Burattine, E. & Simeoni, S. (1994) *Neues Jahr. Mineral. Monatsch.* **5,** 217–229.
21. Perrault, G., Harvey, Y. & Pertsowsky, B. (1975) *Can. Mineral.* **13,** 68–74.
22. Peterson, R. C. & Grey, I. E. (1995) *Can. Mineral.* **33,** 1083–1089.
23. Brindley, G. W. & Brown, G., eds. (1980) *Crystal Structures of Clay Minerals and Their X-ray Identification* (Mineralogical Soc., London), Monograph 5.
24. Bailey, S. W., ed. (1988) *Hydrous Phyllosilicates (Exclusive of Micas)*, Reviews in Mineralogy (Mineralogical Soc. Am., Washington, DC), Vol. 19.
25. Brauner, K. & Preisinger, A (1956) *Folge* **6,** 120–140.
26. Rautureau, M. & Tchoubar, C. (1976) *Clays Clay Miner.* **24,** 43–49.
27. Hawthorne, F. C., Oberti, R., Cannillo, E., Sardone N. & Zanetti, A. (1995) *Am. Mineral.* **80,** 165–172.
28. Yamnova, N. A., Egorov-Tismenko, Yu. K. & Khomyakov, A. P. (1966) *Crystallogr. Rep.* **41,** 257–262.
29. Khomyakov, A. P., Roberts, A., Nechelyustov, G. A. & Pushcharovsky, D. Y. (1996) *Proc. Russ. Mineral. Soc.* **4,** 79–85.
30. Egorov-Tismenko, Yu. K., Yamnova, N. A. & Khomyakov, A. P. (1996) *Crystallogr. Rep.* **41,** 826–830.
31. Ferraris, G., Khomyakov, A. P., Soboleva, S. V. & Belluso, E. (1996) *Acta Mineral. Petrogr.* **37** Suppl., 36.
32. Nicholson, K., Hein, J. R., Bühn, B. & Dasgupta, S. (1996) *Geological Society Special Publication No. 119* (Bath, U.K.).
33. Skinner, H. C. W. & Fitzpatrick, R. W. (1992) *Catena Suppl.* **21.**
34. Tian, Z., Yin, Y., Suib, S. L. & O'Young, C. L. (1997) *Chem. Mater.* **9,** 126–133.
35. Schulze, D., McCay-Buis, T., Sutton, S. R. & Huber, D. R. (1995) *Phytopathology* **59,** 990–994.
36. Illman, B. L. & Dowd, B. A. (1997) *Synchrotron Rad. News* **10,** 18–23.
37. Russell, M. J. & Hall, A. J. (1997) *J. Geol. Soc. London* **154,** 377–402.